***Supporting Information***

# Pyrochlore Nanocrystals as Versatile Quasi-Single-Source Precursors to Lithium Conducting Garnets

*J. Mark Weller*[1] *and Candace K. Chan*[1,2]*

1. Materials Science and Engineering, School for Engineering of Matter, Transport and Energy, Arizona State University, P.O. Box 876106, Tempe, AZ 85827, USA
2. Department of Heterogenous Catalysis, Max-Planck-Institut für Kohlenforschung, Kaiser-Wilhelm-Platz 1, 45470 Mülheim an der Ruhr, Germany

Corresponding author: *candace.chan@asu.edu

## Outline

## 1. Experimental Details

### 1a. Materials and Reagents

All reagents used were of ACS grade or higher unless otherwise noted and used as-received. Lithium nitrate ($LiNO_3$, anhydrous), lithium hydroxide (LiOH, anhydrous), sodium hydroxide (NaOH, anhydrous), zirconium oxychloride octahydrate ($ZrOCl_2 \bullet 8H_2O$), tantalum oxide ($Ta_2O_5$), calcium nitrate tetrahydrate ($Ca(NO_3)_2 \bullet 4H_2O$), and lanthanum nitrate hexahydrate ($La(NO_3)_3 \bullet 6H_2O$) were obtained from Alfa Aesar. Sodium fluoride (NaF) was obtained from Sigma-Aldrich. Potassium hydroxide (KOH, anhydrous) was obtained from Spectrum Chemical. Lithium peroxide ($Li_2O_2$, technical grade, 95%) was obtained from Acros Organics. Methanol (HPLC grade) was obtained from BDH Chemical and de-ionized water (18 MΩ cm, EMD MilliPore NanoPure system) was used in all washing steps.

### 1b. Molten Salt Synthesis of doped pyrochlore-type LZO in eutectic NaOH-KOH

For synthesis of pyrochlores, NaOH and KOH in a eutectic mixture (51.5 : 48.5 by mole) were first pre-heated (5 °C $min^{-1}$) to 400 °C in an $Al_2O_3$ (Coorstek High Alumina, 99.8%, 100 mL, part # 65505) or optionally a $ZrO_2$ (100 mL, AdValueTech, part # Zc-6100) crucible and fully mixed by gentle agitation of the crucible with tongs to form a molten eutectic mixture. The synthesis was performed in air using a KSL-1100x-type compact muffle furnace (MTI Corporation). Meanwhile, $La(NO_3)_3$, $ZrOCl_2$, and optionally dopant sources such as $Ta_2O_5$, $Ca(NO_3)_2$, or NaF were hand ground together using a mortar and pestle with minimal methanol (generally about 1 mL per gram of precursor) to form a fine paste-like mixture which was subsequently dried at elevated temperature (*e.g.* 120 °C) in air to evaporate the methanol and water of hydration, resulting in a foamy, brittle mixture of precursors. Once dried, the precursor mixture was hand ground again into a fine powder.

The ground precursor mixture was then added slowly in small increments (generally 250-500 mg at a time) to the molten hydroxides with intermittent agitation of the melt by grasping the crucible with tongs to ensure uniform mixing of the powders into the melt. To carry out this mixing, the crucible was first removed from the furnace interior and placed on the furnace door to minimize cooling and thermal shock. For this step, the time that the crucible was resting on the open furnace door was minimized to < 30 sec for adding reagents and mixing. If all of the precursors could not be added in < 30 sec, the crucible was returned to the furnace to reheat for at least 30 sec before repeating the precursor addition and mixing process. (In this case, the furnace contains a "drop-down" door that swings downward and so the crucible can be rested upon it; if a furnace with a door that opens horizontally (*i.e.*, swings open/shut like a conventional door) is used, placing the crucible on a refractory fiber plate would be advisable to prevent temperature gradients.)

Once all precursors were added, the melt was agitated one more time to ensure uniformity and placed back into the furnace for the desired hold time (1 h for optimized synthesis). *It should be noted that precursor salts that contain water or may evolve gases (such as from the decomposition of nitrates) should be added to the molten salts* ***slowly*** *and with*

***extreme care*** *to prevent splashing of hot molten salts.* ***Proper protective equipment (e.g., lab goggles that entirely cover the eyes and/or face shield, nitrile gloves, lab coat, heat resistant gloves etc.) is mandatory and all operations should be performed inside of a fume hood behind the fume hood sash to contain evolved gases and also act as a physical barrier in case of any bubbling or splashing of hot molten salts****. Naturally, larger reactions require more care due to the potentially larger amount of gas released from reagent decomposition. Pre-drying of the hydrated precursors is necessary to prevent rapid off-gassing of water vapor, which in turn can cause splashing of the salts. This also motivates addition of reagents in small increments to limit reactivity of the decomposition of nitrates.*

After the synthesis was complete and the mixture cooled, de-ionized water was added to the crucible on top of the solidified hydroxides. The hydroxides were dissolved and the resultant pyrochlore products dispersed by using an immersion ultrasonic horn (Cole-Parmer 500 W Ultrasonic Processor). ***Care must be taken at this stage as the dissolution of hydroxides is highly exothermic. It is recommended to contain the crucible in a larger vessel (e.g. a 500 mL beaker for a 100 mL crucible) filled with water to disperse heat generated by this process.*** After all of the hydroxides were dissolved and a uniform suspension obtained, the pyrochlore nanocrystals were washed by repeated centrifugation steps as follows: 1) the suspension was centrifuged at 8000 RPM until all particles were precipitated, 2) the supernatant solution was decanted and replaced with fresh de-ionized water, 3) the powders were resuspended via the same immersion ultrasonic horn until a uniform suspension was obtained. Then, steps 1-3 were repeated at least 4 more times to remove residual hydroxides and salts. Generally, this process is repeated until the pH of the supernatant solution is less than 10. Finally, the pyrochlores are dried at elevated temperature (e.g. > 120 °C) in air for subsequent use.

As a final note, the NaOH-KOH melt is somewhat corrosive, and in our experience the purity of the $Al_2O_3$ crucible used is crucial. Higher purity and ideally low surface roughness and high-density crucibles minimize adventitious Al-contamination of the pyrochlores originating from corrosion of the crucible. The optimized synthesis time of 1 h as mentioned above helps to minimize Al-dissolution. Although commonly used as a dopant for LLZO, Al-contamination in this process tends to result in poor sintering of the final garnet ceramic. (We do not believe the presence of minor Al-contamination affects the garnet formation process, just the sintering process.) $ZrO_2$ crucibles may also be used as described above, but the susceptibility to thermal shock must be carefully considered. The pyrochlore samples which resulted in the best properties for both conventionally sintered and reactively sintered garnets (including those presented in **Figure 3**) were those synthesized in $ZrO_2$ crucibles at 400 °C for 1 h.

### *1c. Molten Salt Synthesis of LLZTO in $LiNO_3$-$LiOH$-$Li_2O_2$ from doped pyrochlores*

In general, the flux forming salts ($LiNO_3$ and LiOH ~ 1.1 : 3.2 ratio by mole, ~ 1 : 1 ratio by mass) along with a specified amount of $Li_2O_2$ ([0, 0.5, or 1] : 3.2 mole ratio of $Li_2O_2$ : LiOH for total reagent ratios of 1.1 : 3.2 : [0, 0.5, 1.] of $LiNO_3$ : LiOH : [$Li_2O_2$]) were coarsely mixed and heated at a rate of 5 °C $min^{-1}$ in alumina crucibles (Coorstek high alumina (99.8%) 100 mL, part # 65505) and stirred by gently agitating the melt using tongs to ensure homogeneity once the desired hold temperature had been reached. The synthesis was performed in air. Once the salt mixture was molten and at the desired reaction temperature, a thoroughly hand ground mixture of doped pyrochlore nanocrystals and extra $LiNO_3$ (1:1 by mass) was added to the mixture, stirred as before by gentle agitating of the mixture with tongs until a uniform melt was obtained, and held for various times (between 1 – 5 h) at the desired temperature and cooled naturally to room temperature in the furnace. The $LiNO_3$ mixed with the pyrochlore powder is in addition to the fixed molar ratio of $LiNO_3$ : LiOH (1.1 : 3.2) in the melt, and helps facilitate rapid distribution of the pyrochlores in the melt due to the low melting point of $LiNO_3$. Generally batch sizes of ~ 12-15 g total (10:1 to 13:1 ratio of total salts to pyrochlores depending on the amount of $Li_2O_2$ used) were employed for exploratory synthesis and larger batches (up to 4x or ~ 60 g total) were made for testing sintering conditions. A typical small-scale synthesis consisted of 5 g $LiNO_3$, 5 g LiOH, 3 g $Li_2O_2$, and a mixture of 1 g pyrochlore and 1 g $LiNO_3$ (hand ground as described above) as the precursor mixture.

After synthesis, ultrapure water (>18 MΩ cm) was added to the cooled crucibles and the suspension was sonicated using an immersion ultrasonic horn (Cole-Parmer 500 W Ultrasonic Processor) to rapidly dissolve the salts and generate a slurry. Subsequently, the slurry was vacuum filtered using poly(vinylidene fluoride) membranes (0.22 µm pore size, DuraPore, EMD corporation) and washed thoroughly and repeatedly by water followed by a small amount of methanol to facilitate faster drying. For a typical reaction size, 250 mL of de-ionized water are used in total, followed by 50 mL of methanol. Naturally, under-washing or over-washing will result either in residual Li compounds (which can be seen in the XRD patterns as LiOH or $Li_2CO_3$) or excessive protonation of the garnet, but the amounts used here are considered approximately optimized. Finally, the filter membranes along with the wet powder cakes were placed in an oven at > 120 °C and dried in air. After drying, the powders were removed from the filter membranes and lightly ground with a mortar and pestle to de-agglomerate the powder.

### *1d. Solid-State Reaction of LLZTO for Use as Mother Powder*

For use as mother powder for sintering, LLZTO of the same composition as that prepared using the MSS methods was synthesized via the solid-state reaction (SSR) method. Stoichiometric $La(OH)_3$, $ZrO_2$, and $Ta_2O_5$ with 20% excess $Li_2CO_3$ (based on the composition $Li_{6.4}La_3Zr_{1.4}Ta_{0.6}O_{12}$) were used as reagents. The reagents were ball-milled (MSE Supplies benchtop planetary ball-mill, Tucson AZ) in an equivalent mass of 2-propanol using a planetary ball mill. Zirconia jars and milling media were used, and the mill was operated at 700 RPM for 4 h. Subsequently, the milled reagents were collected, and the 2-propanol was evaporated in a fume hood. The powder was transferred to a MgO crucible (Tateho Ozark Technical Ceramics round tray with flanged MgO lid, part # SR3005 for crucible and SF300 for the lid) and calcined once at 1000 °C for 8 h. The synthesis was performed in air. After calcination, the powder was lightly ground with an agate mortar and pestle to de-agglomerate before use.

### *1e. Preparation of Ceramic Pellets*

LLZTO pellets for conventional sintering were consolidated from as-synthesized LLZTO powders via uniaxial cold-pressing (SpecAc Atlas 15T Manual Hydraulic Press) using a 7 mm stainless steel die. Pellets were uniaxially pressed using 125 MPa pressure for 5 minutes at room temperature.

For LLZTO pellets prepared by reactive sintering, doped pyrochlore ($La_{2.4}Zr_{1.12}Ta_{0.48}O_{7.04}$) powders were blended with LiOH (10 % excess by mole relative to target composition of $Li_{6.4}La_3Zr_{1.4}Ta_{0.6}O_{12}$) by ball-milling (SPEX 8000M, polymer jars with tungsten carbide inserts and tungsten carbide milling ball) in a vibratory ball-mill for 90 minutes to ensure uniformity of LiOH throughout the pyrochlore nanocrystals. Subsequently, green pellets were pressed in the same way as described above for LLZTO powder.

Pressed green pellets were sintered at 1200 °C, with 2 hours representing a roughly optimized sintering time. (Some pellets were sintered for 3 h at 1200 °C, with slightly lower ionic conductivity, and were fractured for SEM analysis of the fracture surface, as shown in **Figure 3a,c**.) Sintering was performed in a Thermo Scientific Lindberg Blue M 1700 °C box furnace. All pellets were sintered in MgO crucibles (Tateho Ozark Technical Ceramics) as MgO is known[1,2] to be more inert to LLZO and $Li_2O$ than most other crucible materials besides Pt.

For sintering, pellets were placed on a small bed (10-20 mg) of mother powder (synthesized via conventional solid-state reaction, see ***Sec. 1d*** above and used to prevent stiction between the LLZTO pellet and the substrate) which was placed atop a porous MgO substrate (Tateho Ozark Technical Ceramics, 98.5% MgO grade CTM porous spacer). Additionally, a mixture of mother powder and $Li_2O_2$ was employed (6 : 3 : 1 mass ratio of mother powder : pellet : $Li_2O_2$) and placed below the porous MgO substrate inside of the MgO crucible to provide a $Li_2O$-rich[2] vapor phase (see **Scheme S1a**). The use of a mixture of LLZTO and $Li_2O_2$ inside the sintering crucible was also investigated in our previous work[3] found to be effective for providing a $Li_2O$ source to enable good sintering while minimizing "wasted" LLZTO mother powder. The crucible was covered with a MgO lid (Tateho Ozark Technical Ceramics) during sintering. For these sintering experiments, the smallest crucibles possible were used to minimize evaporation of Li (in our case, 1" diameter and 0.5" tall crucibles, Tateho Ozark part no. SR1005 and SF100).

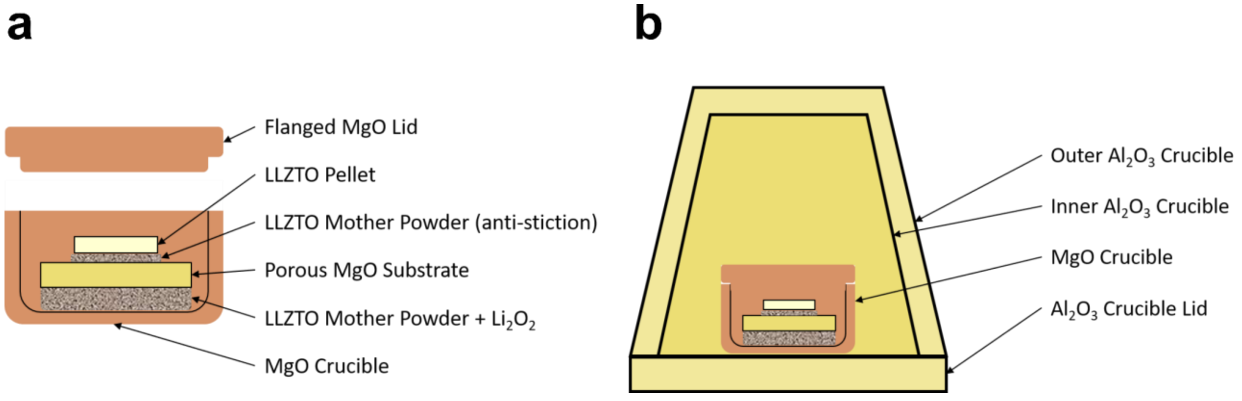

**Scheme S1**. **(a)** arrangement of MgO crucible containing LLZTO pellet for sintering and contain $Li_2O$ vapor, **(b)** arrangement of MgO sintering crucible situated in nested $Al_2O_3$ crucibles to contain further $Li_2O$ vapor and limit egress of $Li_2O$ vapor into furnace atmosphere

The entire MgO crucible assembly was then placed on an $Al_2O_3$ crucible lid and enclosed within inverted larger $Al_2O_3$ crucibles (Coorstek 100 and 250 mL High Alumina crucibles, part no. 65505 and 65506 respectively) for sintering to contain Li-vapor and prevent / minimize interaction with the furnace heating elements (see **Scheme S1b**). We would like to note that excess Li vapor can cause substantial damage to furnace heating elements over time if not contained adequately. The density of the as-sintered pellets was calculated from the sample geometry (measured using a micrometer) and mass and compared to the theoretical density of $Li_{6.4}La_3Zr_{1.4}Ta_{0.6}O_{12}$ (5.5 g $cm^{-3}$).[4]

### *1f. Materials Characterization*

Synchrotron X-ray diffraction (XRD) and pair distribution function (PDF) measurements of the pyrochlore nanocrystals were performed at room temperature at beamline I15-1 of Diamond Light Source (Didcot, UK) with 2D PerkinElmer image plate detectors. Bragg data were collected at $\lambda = 0.161669$ Å and background subtracted using GSAS II.[5] The XRD patterns in **Figure 1a** were scaled to Cu Kα scattering angles for standardization and compared to reference patterns for $La_2Zr_2O_7$ (PDF#00-017-0450) and $La(OH)_3$ (PDF#00-006-0585).

The total scattering data were collected over a Q range of 0.5 – 25 Å$^{-1}$ with $r_{max} = 50$ and $r_{step} = 0.02$ and corrected for multiple scattering, incident beam polarization, and Compton scattering using GudrunX[6] to obtain the PDFs (*D(r)* data as defined by Keen[7]). A sample density of 6.05 g/cm$^3$ was used for the normalizations and $Q_{max} = 25$. PDF refinements and calculations were performed using PDFGui[8] with $Q_{damp} = 0.0267$ and $Q_{broad} = 0.0105$ (obtained from refinement of a Si standard) within the xPDFSuite[9] software package. The scale factor, lattice constant, linear atomic correlation factors *delta1* or *delta2* (coefficients for 1/r or 1/r$^2$ contribution to peak sharpening at high and low temperatures, respectively), *spdiameter* (shape damping function for particle diameter in Å), and isotropic atomic displacement parameters were selected as constraints. For phase identification, the crystallographic information files for pyrochlore (ICSD coll. code 253064) and defect fluorite (ICSD coll. code 253062) were taken from the work by Paul *et al.*[10] The hexagonal form of $La(OH)_3$ was used as reference in PDF refinements (ICSD coll. code 192271, taken from ref.[11]).

Laboratory X-ray diffraction (XRD) of garnet products was performed using a Bruker D-8 powder diffractometer with $CuK_\alpha$ radiation for crystalline phase identification. The reference pattern for c-LLZO ($Ia\bar{3}d$) was generated according to the structure reported by Logeat *et al.*[12]

The sample morphology was examined using a FEI XL30 scanning electron microscope (SEM) equipped with an EDAX system for energy dispersive spectroscopy (EDS). To minimize charging, a carbon film was deposited on the samples before imaging using a thermal evaporator type carbon coater.

Transmission electron microscopy (TEM) was performed using an aberration corrected (CEOS image corrector) FEI Titan Environmental TEM operated at 300 kV. For high-resolution aberration corrected TEM imaging, aberrations were corrected to yield an imaging resolution better than 1 angstrom, and negative spherical aberration imaging (Cs ~ -13 µm) was employed to yield bright contrast at the positions of atom columns. Electron diffraction (ED) patterns were obtained using a third condenser lens to allow formation of a submicrometer diameter parallel beam rather than using a selected area aperture. Scanning transmission electron microscopy (STEM) was performed using a JEOL ARM200 probe-corrected STEM (CEOS CESCOR hexapole probe aberration corrector) with a high-angle annular dark-field (HAADF) detector and JEOL energy dispersive X-ray spectrometer for elemental mapping. To prepare S/TEM samples, pyrochlore or garnet powder was ultrasonically suspended in HPLC-grade methanol. A holey carbon TEM grid (Pacific Grid Tech) was then briefly immersed into the aforementioned suspension. Finally, the grid was dried at elevated temperature (*e.g.*, 120 °C) in air to fully remove methanol. Analysis of elemental maps was performed in part using the Cornell Spectrum Imager plugin in ImageJ.[13]

## 2. Determination of ionic conductivity from EIS data

After sintering, the pellets were polished successively using 240, 400, 1200, and 2000 grit silicon carbide polishing films (MTI) until a smooth, uniform, and reflective surface was obtained. To prepare non-blocking electrodes, Li-foil (Sigma-Aldrich) and Sn-foil (Alfa Aesar) were first melted at 250 °C in a stainless-steel cup on a laboratory hot plate in an Ar-filled glovebox to form a 20 wt% Sn-Li alloy (~ 1.5 mol% Sn) as demonstrated by Wang *et al.*[14] Subsequently, both sides of the 2000 grit polished LLZTO pellets were contacted with the molten Sn-Li alloy for 30 – 60 seconds (with mild rubbing of the pellet in the molten alloy to ensure that any surface contaminants weren't sticking to the pellet) to result in a well-adhered film. This process was repeated for each side of the pellet. These pellets were subsequently characterized via EIS using a SP-200 potentiostat from Biologic.

Fitting of EIS data was performed using EC-Lab v.11.33 software from Biologic. The circuit ($\mathbf{R}_b/\mathbf{Q}_b$)($\mathbf{R}_{gb}/\mathbf{Q}_{gb}$)($\mathbf{R}_{el}/\mathbf{Q}_{el}$)($\mathbf{Q}_{lf}$) is commonly used for fitting EIS spectra from garnet electrolytes, where 'b,' 'gb,' 'el,' and 'lf' are 'bulk', 'grain boundary', 'electrode', and 'low-frequency' respectively.[15] For our samples, no appreciable grain boundary impedance (generally the maximum grain boundary semicircle is observed at frequencies in the 10's of kHz)[15] was observed, so the circuit ($\mathbf{R}_{tot}/\mathbf{Q}_{tot}$)($\mathbf{R}_{el}/\mathbf{Q}_{el}$)($\mathbf{Q}_{lf}$) was used instead for fitting impedance spectra with Sn-Li electrodes, where 'tot,' 'el,' and 'lf' are the 'total,' 'electrode,' and 'low-frequency' components to impedance respectively. The total ionic conductivity, σ (S $cm^{-1}$), was determined from the $R_{tot}$ values, the pellet thickness (*t*), and the pellet cross-sectional area (*A*) per Equation S1.

$$\sigma = \frac{t}{R_{tot}A} \qquad \text{(S1)}$$

Additionally, the temperature dependence of ionic conductivity was investigated for these pellets at various temperatures between 273-343 K in order to determine the activation energy of Li-ion conduction ($E_a$) based on the Arrhenius equation (Equation S2).

$$\sigma \propto e^{\frac{-E_a}{k_b T}} \qquad \text{(S2)}$$

Impedance measurements at various temperatures were performed by placing the LLZTO sample in a sealed pouch cell (foil poly bag sealed with an impulse sealer) with strips of copper foil attached as current collectors such that part of the foil extended out of the sealed poly bag in order to allow measurements outside of an inert atmosphere as in our previous work.[3] Copper tape was attached to the copper foils to make more mechanically robust connections. For temperatures above room temperature, a temperature-controlled oven (Thermo Scientific HeraTherm) with a thermostat was used. For measurements at 273 K, the sealed pouch containing the LLZTO pellet-electrode assembly was placed in a polymer bag, which was in turn immersed in an ice bath (EMD Millipore NanoPure system used to provide pure water). By virtue of immersion in the ice-water bath, air was removed from the polymer bag providing good thermal contact between the cold bath and the sealed LLZTO pellet-electrode assembly. For measurements at a new temperature, at least 10 minutes were given for thermal equilibration after the temperature readout on the oven thermostat or ice bath thermocouple reached the desired temperature. A linear regression of ln (σ) vs. $T^{-1}$ was performed to determine the value of $E_a$ based on the slope of the line.

## 3. Supporting Tables

**Table S1**. Experimental conditions for synthesis of $Li_{6.4}La_3Zr_{1.4}Ta_{0.6}O_{12}$ garnet from $La_{2.4}Zr_{1.12}Ta_{0.48}O_{7.04}$ pyrochlore quasi-single-source precursors with corresponding reaction products as determined from the XRD patterns in **Figure S2**. The temperature, reaction time, and $Li_2O_2$ : LiOH molar ratio was varied (the molar ratio of $LiNO_3$ to LiOH was fixed at 1.1 to 3.2). As the $Li_2O_2$ to LiOH ratio increases, the Lux-Flood basicity of the melt increases. Some products showing residual LiOH and/or $Li_2CO_3$ in the XRD patterns are considered phase-pure garnet as minor residual LiOH originates from incomplete washing after the synthesis rather than incomplete conversion to garnet, and $Li_2CO_3$ likewise can form from residual this LiOH.

| Reaction Temperature (°C) | $Li_2O_2$ : LiOH (x : 3.2) Molar Ratio | Reaction Time (h) | Reaction Products |
|---|---|---|---|
| 400 | 0 | 5 | Pyrochlore, no garnet |
| | 0.5 | 3 | Garnet with $LiTaO_3$ and $La_2O_3$ |
| | 0.5 | 5 | Garnet with $LiTaO_3$ |
| | 1 | 1 | Garnet with $LiLaO_2$, $LiTaO_3$ and $La_2O_3$ |
| | 1 | 3 | Garnet with $LiTaO_3$ |
| | 1 | 5 | **Pure garnet** |
| 450 | 0.5 | 3 | Garnet with $LiTaO_3$ |
| | 0.5 | 5 | Garnet with $LiLaO_2$, $LiTaO_3$ and $La_2O_3$ |
| | 1 | 1 | Garnet with $LiLaO_2$, $LiTaO_3$ and $La_2O_3$ |
| | 1 | 3 | **Pure garnet** |
| 500 | 0 | 5 | Pyrochlore, trace garnet |
| | 0.5 | 1 | Pyrochlore, no garnet |
| | 0.5 | 3 | **Pure garnet** |
| | 0.5[a] | 3 | Pyrochlore, no garnet |
| | 0.5[b] | 3 | **Garnet** with trace $LiAlO_2$ |
| | 1 | 1 | **Pure garnet** |
| 550 | 0 | 5 | Pyrochlore, $LiTaO_3$, some garnet |
| | 0.5 | 1 | Pyrochlore, some garnet |
| | 0.5 | 3 | **Pure garnet** |
| | 1 | 1 | **Pure garnet** |
| | 1[c] | 1 | **Garnet** with trace $LaAlO_3$ |
| | 1[d] | 4 | **Pure garnet** |

[a] *$Na_2O_2$ used instead of $Li_2O_2$; i.e., 1.1 : 3.2 : 0.5 mole ratio of $LiNO_3$ : LiOH : $Na_2O_2$*

[b] *$Li_{6.025}La_{2.75}Ca_{0.25}Zr_{1.4}Ta_{0.6}O_{11.375}F_{0.625}$ (LLCZTOF) (see **Figure S7**)*

[c] *$Li_{6.375}La_3Zr_2O_{11.375}F_{0.625}$ (LLZOF) (see **Figure S6**)*

[d] *Garnet synthesis using $La(NO_3)_3$, $ZrOCl_2$, and $Ta_2O_5$ as reagents instead of pyrochlores (see **Figure S3**)*

**Table S2**. Z-Fit parameters (tot = total, el = electrode, lf = low-frequency) and pellet properties (A = area, t = thickness, ρ = relative density) and from fitting the total and electrode impedances for pellets of LLZTO from pyrochlore to garnet conventional and reactive sintering measured at room temperature (21 °C) between 7 MHz and 1 Hz with 1.5 mol % Sn-Li electrodes (conductivity in mS cm$^{-1}$).

| MSS Medium | $R_{tot}$ (Ω) | $Q_{tot}$ (F s$^{(a-1)}$) | $R_{el}$ (Ω) | $Q_{el}$ (F s$^{(a-1)}$) | $Q_{lf}$ (F s$^{(a-1)}$) | A (cm$^2$) | t (cm) | $\sigma_{tot}$ (mS cm$^{-1}$) | ρ (%) |
|---|---|---|---|---|---|---|---|---|---|
| **Conventional** | 532 | 2.5 x 10$^{-10}$ | 396 | 1.77 x 10$^{-6}$ | 6.03 x 10$^{-3}$ | 0.299 | 0.0668 | 0.42 | 88 |
| **Reactive** | 660 | 1.61 x 10$^{-10}$ | 1024 | 1.04 x 10$^{-6}$ | 2.33 x 10$^{-3}$ | 0.227 | 0.0793 | 0.53 | 94.1 |

**Table S3**. Comparison of properties of the LLZTO ($Li_{6.4}La_3Zr_{1.4}Ta_{0.6}O_{12}$ unless otherwise noted) prepared using the pyrochlore to garnet (PG) process with other pertinent literature. The synthesis conditions, sintering conditions, relative density, total ionic conductivity ($\sigma_{tot}$, at room temperature unless otherwise indicated) and activation energy ($E_a$) are shown for comparison.

| Synthesis Method | Synthesis Conditions | | Sintering Conditions | | Pellet Properties | | | Ref. |
|---|---|---|---|---|---|---|---|---|
| | Temp. (°C) | Time (h) | Temp.(°C) | Time (h) | Density (%) | **$\sigma_{tot}$** | Ea | |
| Highly-Basic-MSS<br>($LiNO_3$ : LiOH : $Li_2O_2$<br>0.5 : 1 : 1) | 550 | 2.5 | 1200 | 3 | 93.4 | **0.35** | 0.39 | Ref.[16] |
| Modified Highly-Basic-MSS<br>($LiNO_3$ : LiOH : $Li_2O_2$<br>1.1 : 3.2 : 1) | 550 | 8 | 1200 | 4 | 91.1 | **0.61** | 0.4 | Ref.[16] |
| PG-Conventional Sintering | 550 | 1 | 1200 | 2 | 88.0 | **0.42** | 0.42 | This Work |
| PG-Reactive Sintering | N/A | N/A | 1200 | 2 | 94.1 | **0.53** | 0.38 | This Work |
| Mixed-MSS (LiCl-LiOH) | 900 | 4 | 1200 | 2 | 78.5 | **0.45** | NR | Ref.[16] |
| Chloride-MSS (LiCl-KCl) | 900 | 4 | 1200 | 4 | 87.9 | **0.46** | 0.4 | Ref[16] |
| Solid-state reaction$^{*}$ | 900 | 2x10 | 1130 | 36 | 94.1 | $0.28^{b}$ | NR | Ref.[17] |
| Solid-state reaction$^{\ddagger,*}$ | 950 | 2x6 | 1250 | 6 | 93.9 | 0.42 | 0.43 | Ref.[18] |
| Solid-state reaction$^{\ddagger,*}$ | 950 | 2x6 | 1280/1180 | 0.33/5 | 97 | 0.74 | 0.42-0.45 | Ref.[4] |
| Solid-state reaction$^{\ddagger,*}$ | 950 | 2x6 | 1280 | 5 | 97 | 0.78 | 0.42-0.45 | Ref.[4] |
| Solid-state reaction$^{\ddagger,*}$ | 950 | 2x6 | 1250 | 0.33 | 97 | 0.64 | ~0.45 | Ref.[2] |
| Solid-state reaction$^{\ddagger}$ | 900 | 12 | 1180 | 12 | 91 | 0.33 | 0.53 | Ref.[19] |
| Solid state reaction | 900 | 6 | 1200 | 24 | 84 | $0.15^{\ddagger}$ | 0.40 | Ref.[20] |
| Solid state reaction$^{\ddagger}$ | 900 | 6 | 1100 | 15 | 89 | 0.61 | 0.40 | Ref.[21] |
| Solid state reaction$^{\ddagger}$ | 900 | 6 | 1150 | 15 | 92.8 | $0.79^{b,\dagger}$ | 0.42 | Ref.[22] |
| Solid state reaction | 750 | 1x 6, 1 x 12 | $1200^{Al}$ | 18 | 83 | $0.3^{c,\dagger}$ | 0.38 | Ref.[23] |
| Solid state reaction | 900 | 6 | $1150^{Al}$ | 12 | NR | 0.41 | 0.3 | Ref.[24] |
| Solid state reaction$^{*}$ | 1x at 850 /<br>2x at 1000 | 3x20 | $1150^{Al}$ | 5 | 92.7 | $0.71^{c}$ | 0.42 | Ref.[25] |
| Solid state reaction** | 900 | NR | $1140^{Al}$ | 16 | NR | 1.0 | 0.35 | Ref.[26] |
| Co-precipitation | 900 | 3-4 | $1050^{hp}$ | 1 | 97.1 | $0.39^{a}$ | 0.45 | Ref.[27] |
| Co-precipitation | 900 | 3-4 | $1050^{hp}$ | 1 | 97.8 | $0.82^{b}$ | 0.43 | Ref.[27] |

| | | | | | | | | |
|---|---|---|---|---|---|---|---|---|
| Solution-combustion synthesis | 750 | 8 | 1125 | 6 | NR | 0.2 | NR | Ref.[28] |
| Polymer combustion | 700 | 4 | 1100 | 12 | 93.6 | 0.67 | 0.42 | Ref.[3] |

‡ - $\sigma_{tot}$ *measured at 33 °C*
† - $\sigma_{tot}$ *measured at 27 °C*
*a – x = 0.75*
*b - x = 0.5*
*c - x = 0.4*
*hp – consolidated via hot-pressing*
*Al –* $Al_2O_3$ *crucibles used or* $Al_2O_3$ *added as sintering aid*
∤ *- high energy ball milling (e.g. planetary milling, attrition milling, etc.) of LLZTO to reduce particle size*
** - repeated grinding and heating steps (e.g. 2x10 = 2 calcination steps each for 10 hours)*
*** - exact details of synthesis not reported (e.g. degree method of grinding, calcination time, etc.)*
*NR – not reported*

## 4. Supporting Figures

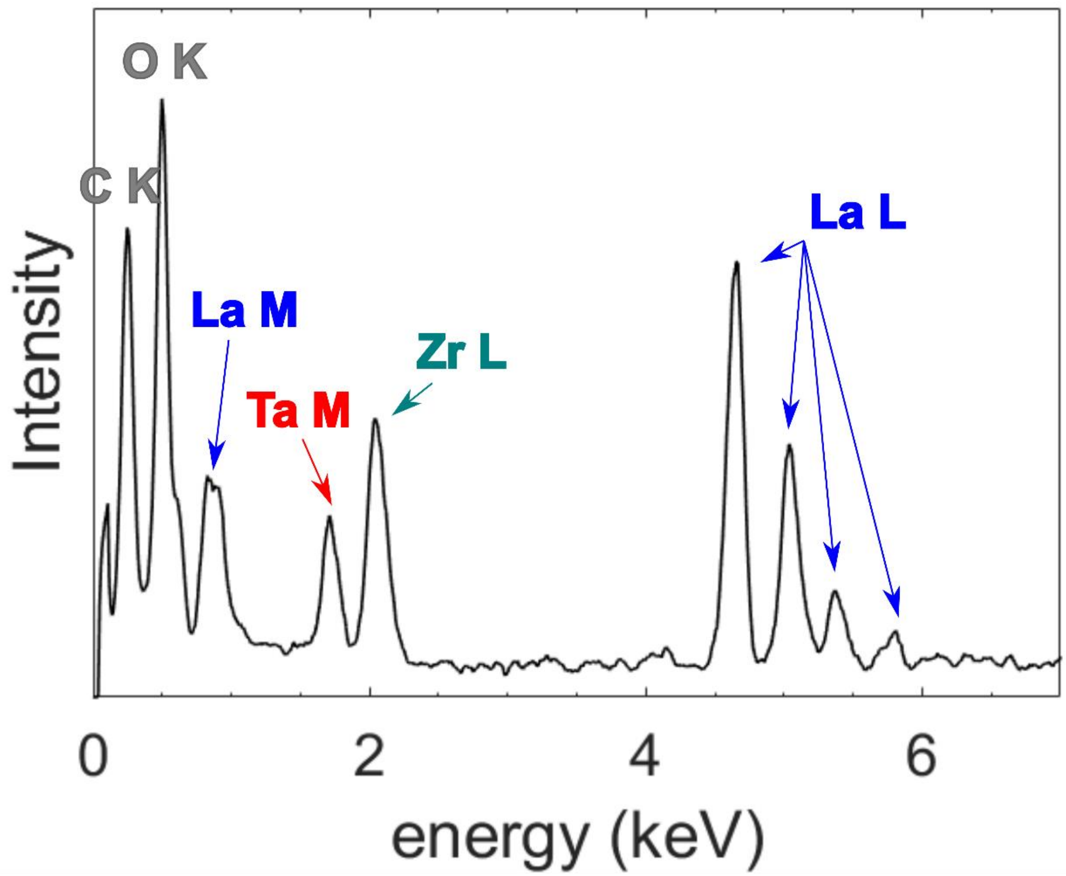

**Figure S1**. Average STEM-EDS spectrum obtained from EDS spectral map in **Figure 1e** for doped pyrochlore precursors with nominal composition of $La_{2.4}Zr_{1.12}Ta_{0.48}O_{7.04}$

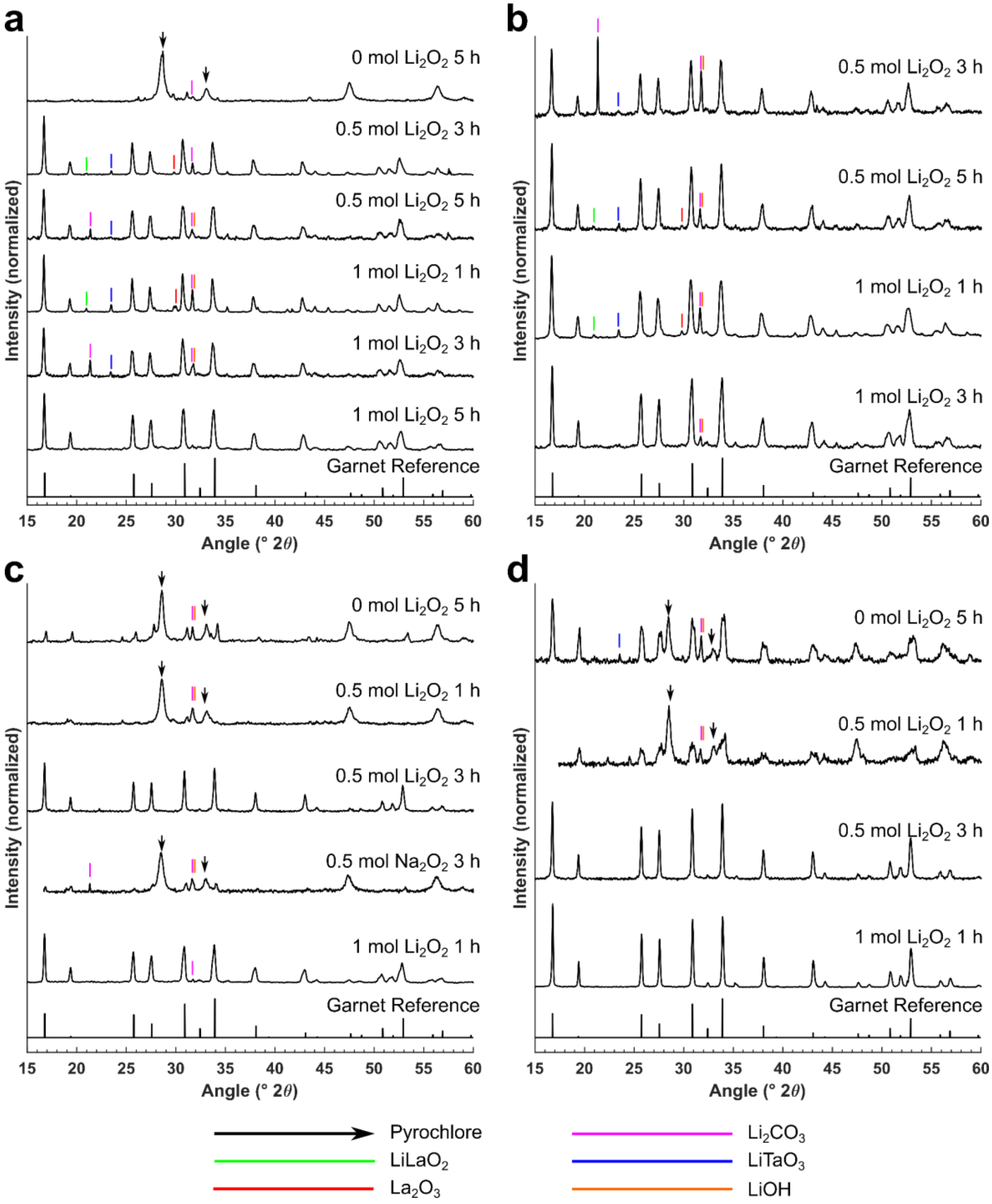

**Figure S2**. XRD patterns of garnets synthesized from pyrochlore precursors at **(a)** 400 °C, **(b)** 450 °C, **(c)** 500 °C, and **(d)** 550 °C. The molar ratio of $Li_2O_2$ to LiOH ($LiNO_3$ to LiOH molar ratio was fixed at 1.1 to 3.2) and reaction time for synthesis are next to each XRD pattern. The reference pattern (Logéat et al.[12]) for garnet is shown below. Main impurity phases besides unreacted pyrochlores (PDF#00-017-0450) are assigned to $LiLaO_2$ (mp-756544[29]), $Li_2CO_3$ (ICSD Coll. Code 69133), $LiTaO_3$ (PDF#00-029-0836), $La_2O_3$ (PDF#00-005-0602), and LiOH (ICSD Coll. Code 27543) as indicated by the vertical lines above major reflections from each phase.

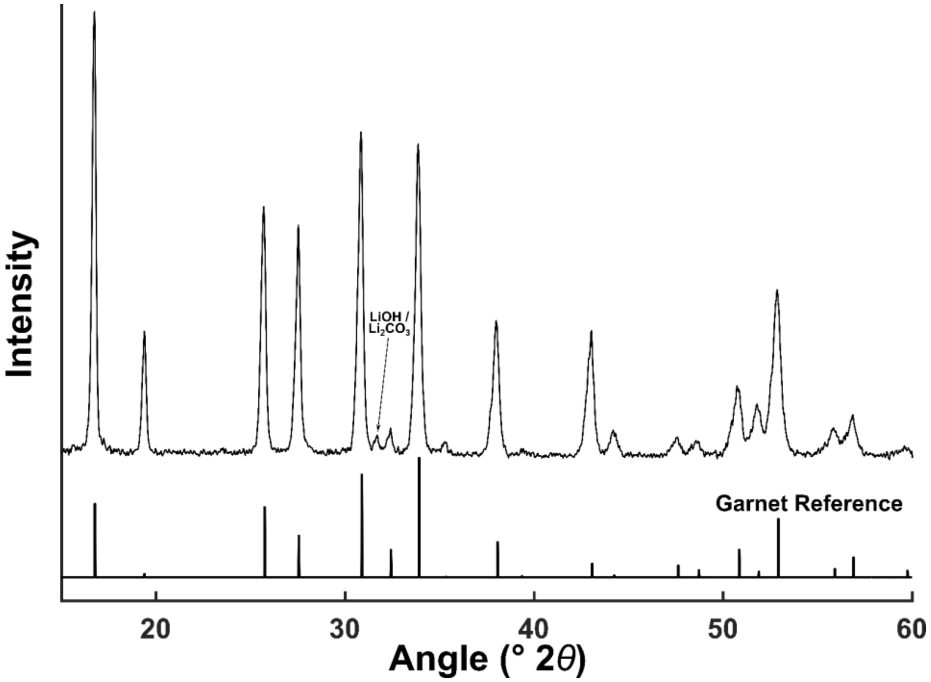

**Figure S3**. XRD pattern of $Li_{6.4}La_3Zr_{1.4}Ta_{0.6}O_{12}$ (LLZTO) garnet powder synthesized using $La(NO_3)_3$, $ZrOCl_2$, and $Ta_2O_5$ as precursors instead of doped pyrochlore nanocrystals at 550 °C in 4 h (reference pattern generated according to Logéat et al.[12]). The salt melt was $LiNO_3$-LiOH-$Li_2O_2$ at a molar ratio of 1.1 : 3.2 : 1. Lower synthesis temperatures resulted in only partial garnet formation. For this sample, the same synthetic approach as outlined in the **Experimental Details, Section 1c** was used, except instead of the doped pyrochlores, a ground mixture of the aforementioned reagents was used as described in our previous[16] work.

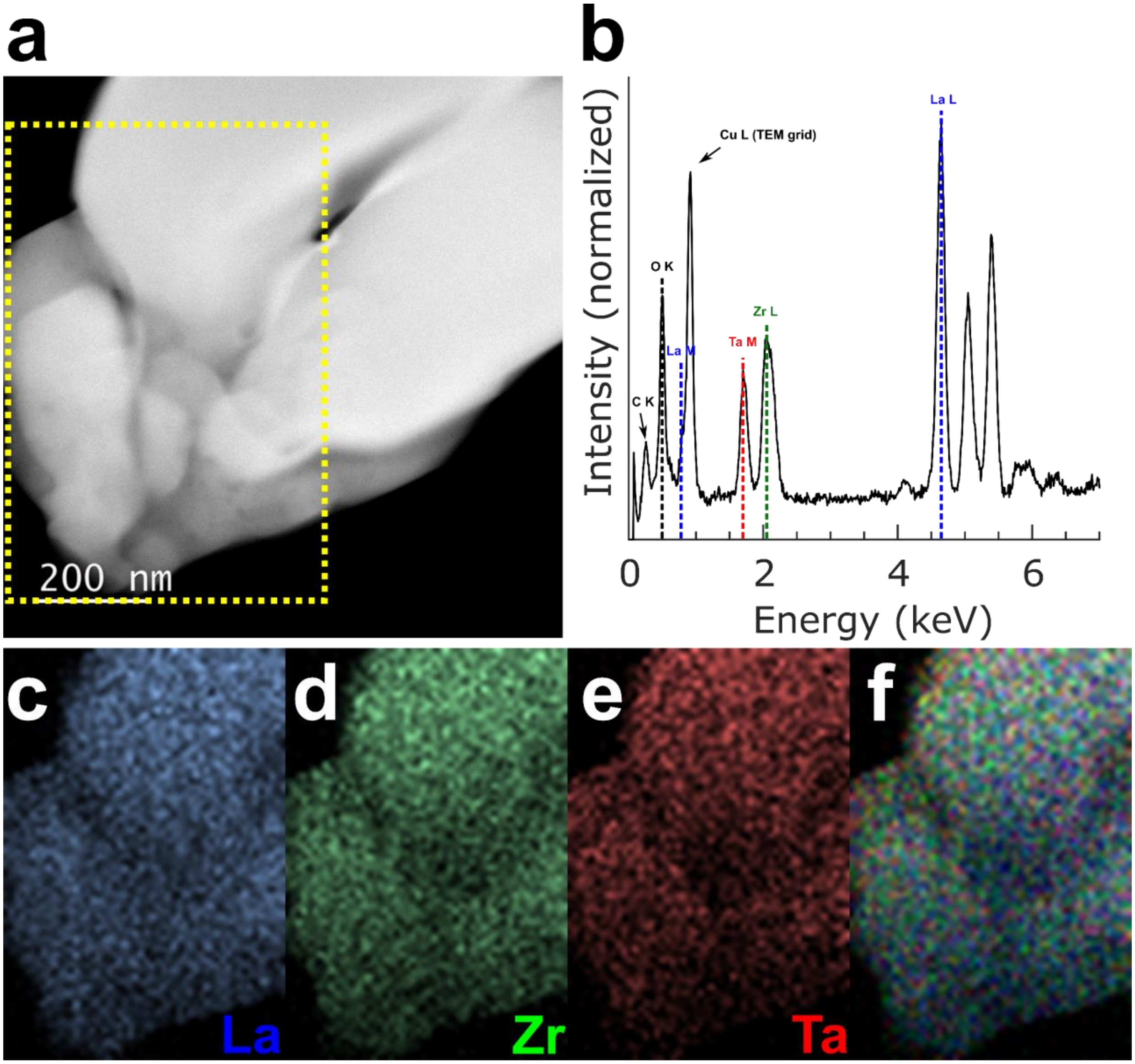

**Figure S4**. TEM analysis of a cluster of garnet particles with nominal composition of $Li_{6.4}La_3Zr_{1.4}Ta_{0.6}O_{12}$ (LLZTO) synthesized from $La_{2.4}Zr_{1.12}Ta_{0.48}O_{7.04}$ pyrochlore precursors. **(a)** HAADF-STEM image with region of interest shown as dotted box, **(b)** average STEM-EDS spectrum and EDS maps of **(c)** La L, **(d)** Zr L, **(e)** Ta M, **(f)** RGB composite image of particle cluster in **(a).**

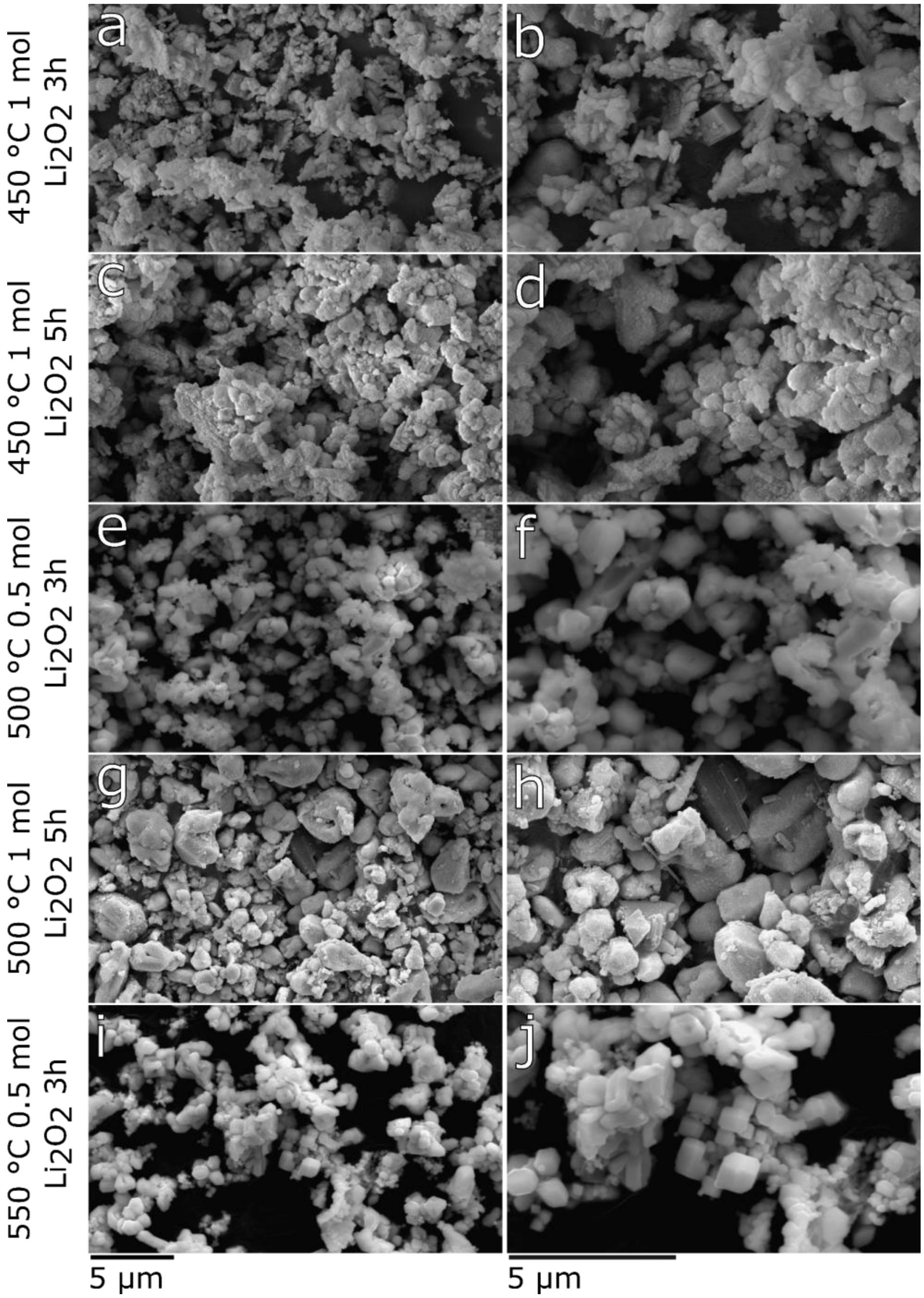

**Figure S5**. SEM images of LLZTO synthesized from doped pyrochlores in ternary basic molten salts ($LiNO_3$:LiOH:$Li_2O_2$ ratio of 1.1:3.2:[0.5 , 1]) at **a,b)** 450 °C, 3 h, 1 moles $Li_2O_2$, **c,d)** 450 °C, 5 h, 1 moles $Li_2O_2$, **e,f)** 500 °C, 3 h, 0.5 moles $Li_2O_2$, **g,h)** 500 °C, 5 h, 1 moles $Li_2O_2$, **i,j)** 550 °C, 3 h, 0.5 moles $Li_2O_2$. Note that some samples were sputtered with Au to minimize charging, which is the source of the texture on the surface of many particles. In general, submicrometer particles result under minimum reaction time conditions (**a-f,i-j**), which have similar size (< 1 µm) and morphology to the powder in **Figure 2b**. However, when the reaction time is extended (**g,h**), the particle size coarsens considerably ( > 1 µm).

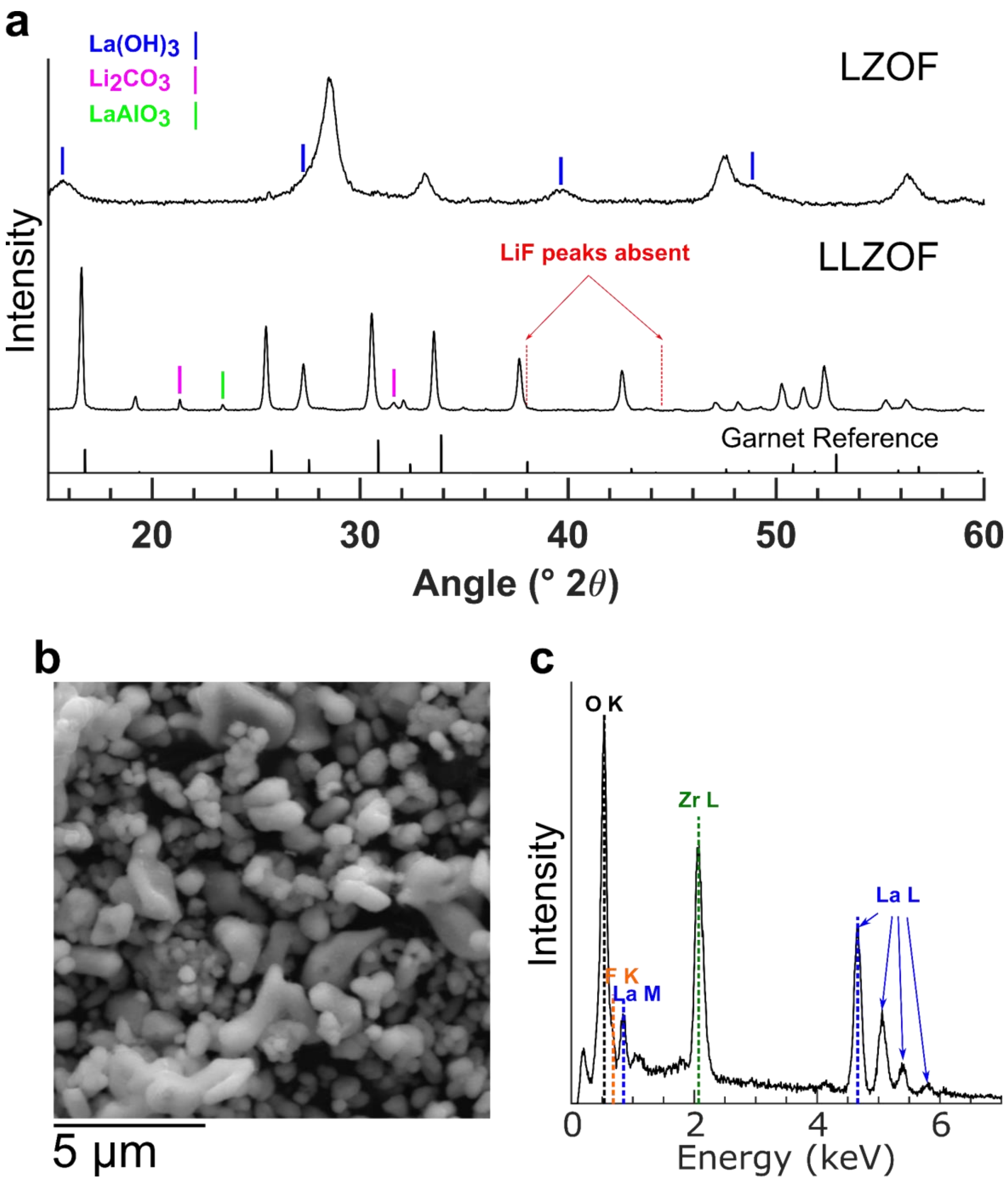

**Figure S6**. **(a)** XRD patterns of $La_{2.4}Zr_{1.6}O_{6.55}F_{0.5}$ pyrochlore (LZOF) synthesized at 400 °C for 4 hours (using $La(NO_3)_3$, $ZrOCl_2$, and NaF as reagents) and $Li_{6.375}La_3Zr_2O_{11.375}F_{0.625}$ (LLZOF) garnet synthesized using the pyrochlore as reagent (reaction with 1 : 3.2 moles $Li_2O_2$ : LiOH at 550 °C for 1 hour) with cubic garnet reference (from Logéat *et al*.[12]) and trace $LaAlO_3$ (ICSD coll. code 92521) noted, which is believed to be a contaminant phase from a worn $Al_2O_3$ crucible, (which can be a challenge as noted in the **Experimental Details 1b** above), note the absence of LiF peaks (ICSD coll. code 41409) indicating incorporation of $F^-$ into the garnet lattice; **(b)** SEM image and **(c)** SEM-EDS spectrum of LLZOF garnet powders synthesized from LZOF pyrochlores with La, Zr, O, and F signals indicated

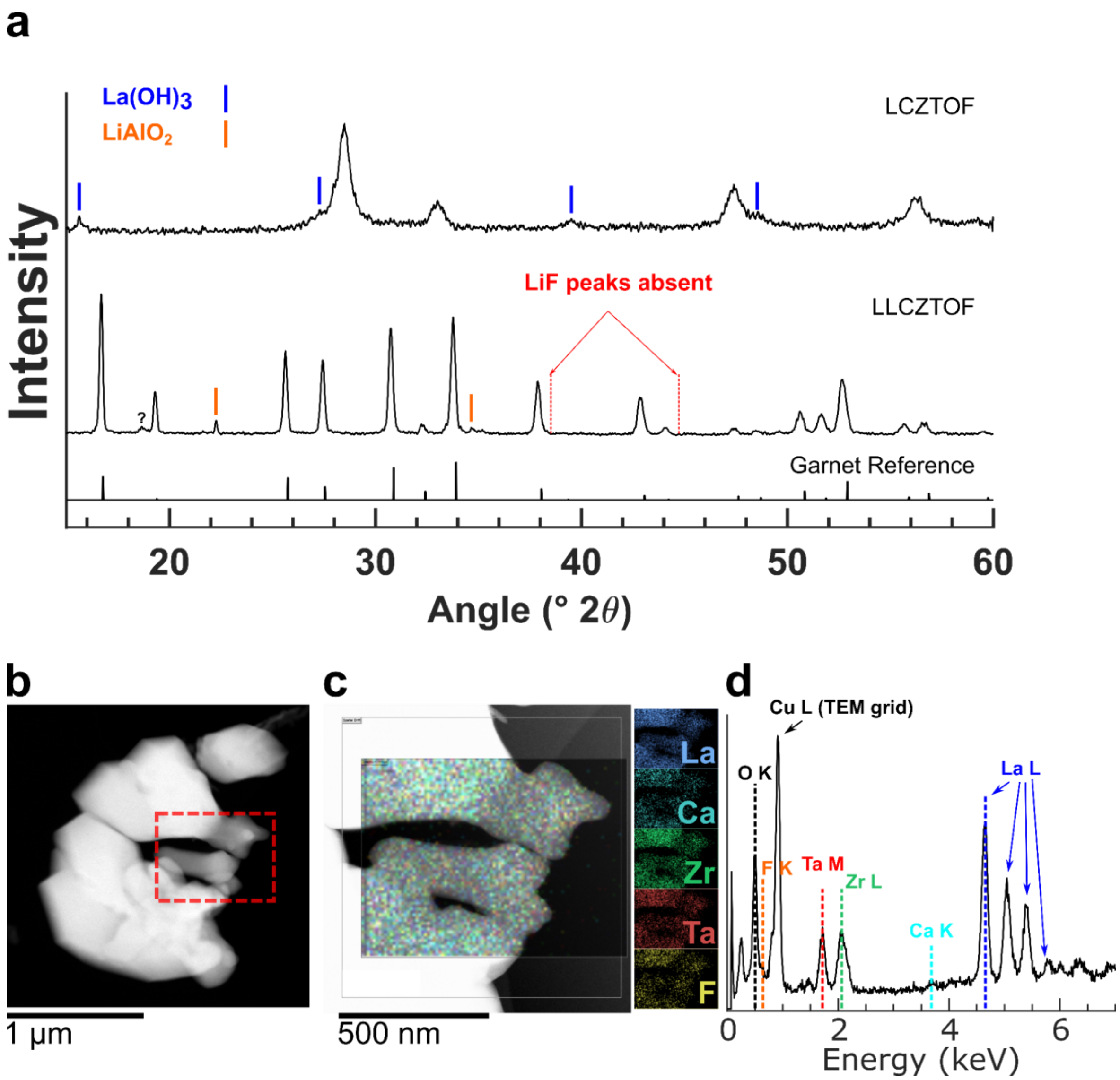

**Figure S7**. **(a)** XRD patterns of pyrochlore synthesized at 400 °C for 4 hours (using $La(NO_3)_3$, $ZrOCl_2$, NaF, and $Ca(NO_3)_2$ as reagents) with nominal composition of $La_{2.2}Ca_{0.2}Zr_{1.12}Ta_{0.48}O_{6.69}F_{0.5}$ (LCZTOF) and garnet with nominal composition of $Li_{6.025}La_{2.75}Ca_{0.25}Zr_{1.4}Ta_{0.6}O_{11.375}F_{0.625}$ (LLCZTOF) synthesized at 500 °C for 3 h (0.5 : 3.2 mol ratio $Li_2O_2$ : LiOH) from the LCZTOF multiply-doped pyrochlore with cubic garnet reference (Logéat et al.[12]) and trace impurity, in this case $LiAlO_2$ (ICSD Coll. Code 23815) noted, which is believed to be a contaminant phase from a worn $Al_2O_3$ crucible, (which can be a challenge as noted in the **Experimental Details 1b** above), note the absence of LiF peaks (ICSD Coll. Code 41409) indicating incorporation of $F^-$ into the garnet lattice, **(b)** HAADF-STEM image of LLCZTOF garnet (region of interest for spectral mapping outlined in red), **(c)** HAAD-STEM image of (**b**) with EDS spectral mapping noted, and individual element maps shown, **(d)** average STEM-EDS spectrum from (**c**) with La, Ca, Zr, Ta, O, and F signals noted.

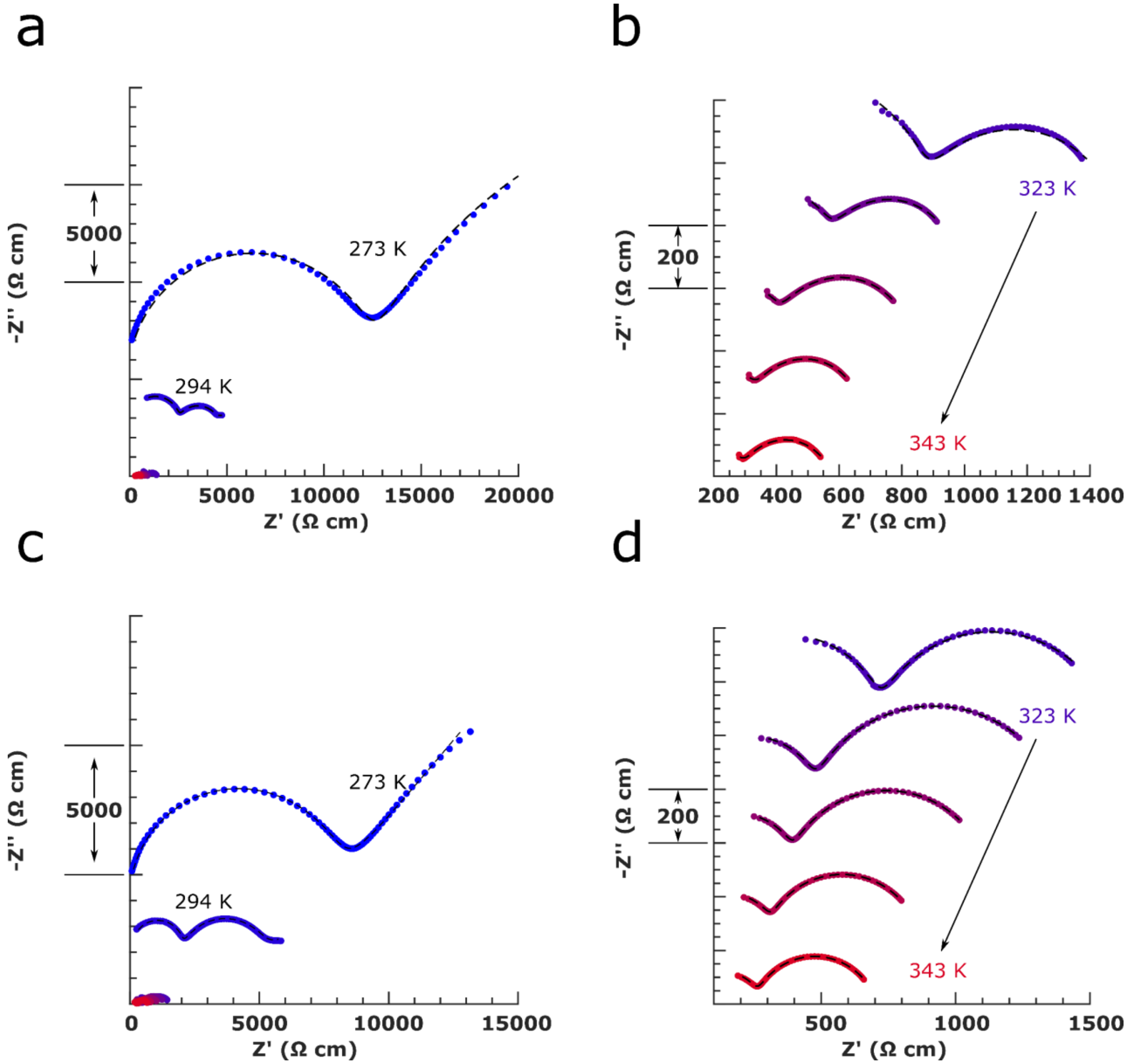

**Figure S8**. Nyquist plots of temperature dependence of impedance used to generate Arrhenius plot in **Figure 3** for conventional sintering, **a)** overview and **b)** zoomed region of (**a**) showing higher temperature EIS spectra, and reactive sintering, **c)** overview and **d)** zoomed region of (**c**) showing higher temperature EIS spectra. Black dashed lines show circuit fitted impedance spectra. For clarity, impedance spectra are vertically offset, major axis marks on -*Z*" axis are shown.

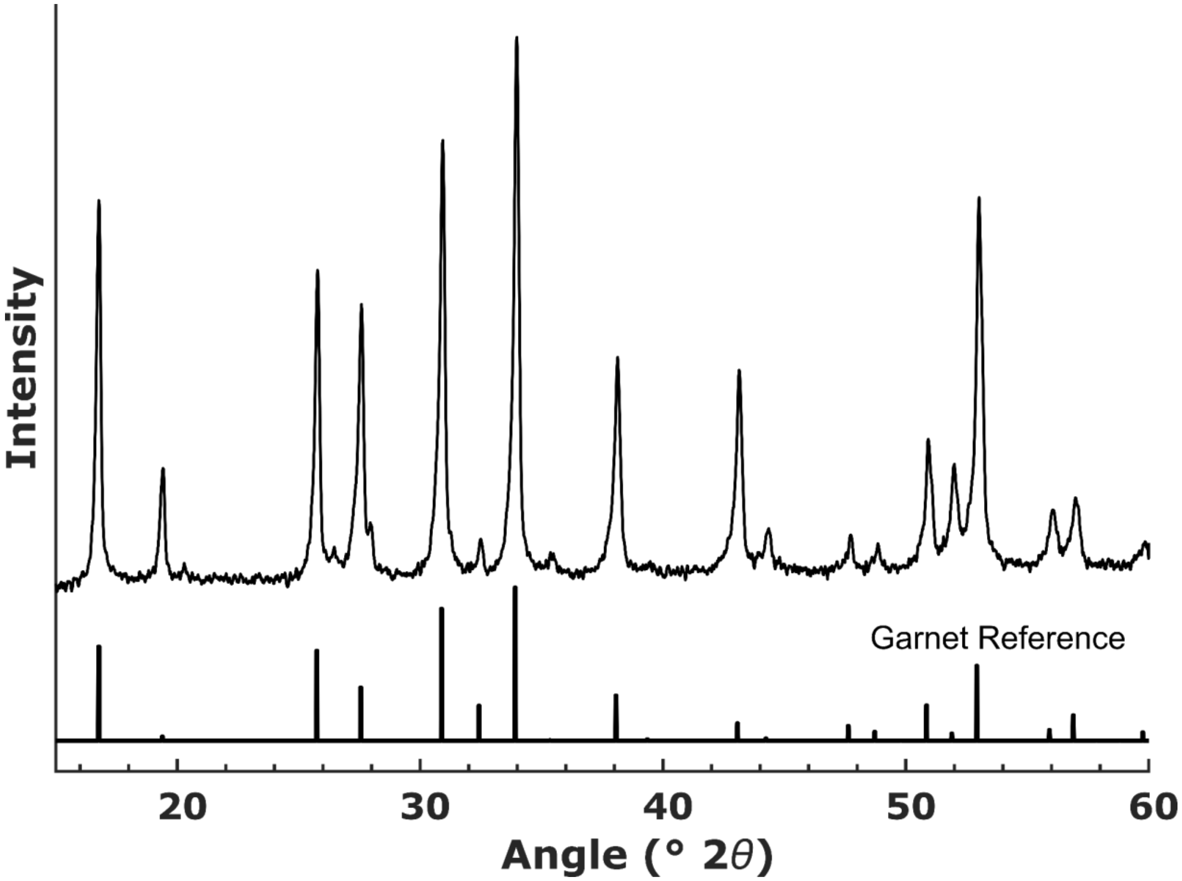

**Figure S9**. XRD pattern of garnet pellet obtained from *in situ* reactive sintering of pyrochlores + LiOH at 1200 °C for 3 h with cubic garnet reference pattern (from Logéat *et al.*[12]) also shown.

## 5. References

1 X. Huang, Y. Lu, H. Guo, Z. Song, T. Xiu, M. E. Badding and Z. Wen, *ACS Appl. Energy Mater.*, 2018, **1**, 5355–5365.

2 X. Huang, Y. Lu, Z. Song, K. Rui, Q. Wang, T. Xiu, M. E. Badding and Z. Wen, *Energy Storage Mater.*, 2019, **22**, 207–217.

3 J. M. Weller, J. A. Whetten and C. K. Chan, *ACS Appl. Mater. Interfaces*, 2020, **12**, 953–962.

4 X. Huang, T. Xiu, M. E. Badding and Z. Wen, *Ceram. Int.*, 2018, **44**, 5660–5667.

5 B. H. Toby and R. B. Von Dreele, *J. Appl. Crystallogr.*, 2013, **46**, 544–549.

6 A. Soper, *GudrunN and GudrunX, Tech. Rep. RAL-TR13, Rutherford Appleton Laboratory*, 2012.

7 D. A. Keen, *J. Appl. Crystallogr.*, 2001, **34**, 172–177.

8 C. L. Farrow, P. Juhas, J. W. Liu, D. Bryndin, E. S. Boin, J. Bloch, T. Proffen and S. J. L. Billinge, *J. Phys. Condens. Matter*, 2007, **19**, 335219.

9 X. Yang, P. Juhas, C. L. Farrow and S. J. L. Billinge, xPDFsuite: an end-to-end software solution for high throughput pair distribution transformation, visualization and analysis. arXiv: 1402.3163 2014.

10 B. Paul, K. Singh, T. Jaroń, A. Roy and A. Chowdhury, *J. Alloys Compd.*, 2016, **686**, 130–136.

11 V. Đorđević, Ž. Antić, M. G. Nikolić and M. D. Dramićanin, *J. Phys. Chem. Solids*, 2014, **75**, 276–282.

12 A. Logéat, T. Köhler, U. Eisele, B. Stiaszny, A. Harzer, M. Tovar, A. Senyshyn, H. Ehrenberg and B. Kozinsky, *Solid State Ionics*, 2012, **206**, 33–38.

13 R. Hovden, P. Cueva, J. A. Mundy and D. A. Muller, *Micros. Today*, 2013, **21**, 40–44.

14 C. Wang, H. Xie, L. Zhang, Y. Gong, G. Pastel, J. Dai, B. Liu, E. D. Wachsman and L. Hu, *Adv. Energy Mater.*, 2018, **8**, 1701963.

15 W. E. Tenhaeff, E. Rangasamy, Y. Wang, A. P. Sokolov, J. Wolfenstine, J. Sakamoto and N. J. Dudney, *ChemElectroChem*, 2014, **1**, 375–378.

16 J. M. Weller and C. K. Chan, *ACS Appl. Energy Mater.*, 2020, **3**, 6466–6475.

17 Y. Wang and W. Lai, *Electrochem. Solid-State Lett.*, 2012, **15**, A68.

18 X. Huang, Y. Lu, J. Jin, S. Gu, T. Xiu, Z. Song, M. E. Badding and Z. Wen, *ACS Appl. Mater. Interfaces*, 2018, **10**, 17147–17155.

19 M. Yi, T. Liu, X. Wang, J. Li, C. Wang and Y. Mo, *Ceram. Int.*, 2019, **45**, 786–792.

20 N. Janani, S. Ramakumar, S. Kannan and R. Murugan, *J. Am. Ceram. Soc.*, 2015, **98**, 2039–2046.

21 R. Inada, K. Kusakabe, T. Tanaka, S. Kudo and Y. Sakurai, *Solid State Ionics*, 2014, **262**, 568–572.

22 R. Inada, S. Yasuda, M. Tojo, K. Tsuritani, T. Tojo and Y. Sakurai, *Front. Energy Res.*, 2016, **4**, 1–12.

23 L. Dhivya and R. Murugan, *ACS Appl. Mater. Interfaces*, 2014, **6**, 17606–17615.

24 M. Huang, M. Shoji, Y. Shen, C. W. Nan, H. Munakata and K. Kanamura, *J. Power Sources*, 2014, **261**, 206–211.

25 C.-L. L. Tsai, V. Roddatis, C. V. Chandran, Q. Ma, S. Uhlenbruck, M. Bram, P. Heitjans and O. Guillon, *ACS Appl. Mater. Interfaces*, 2016, **8**, 10617–10626.

26 Y. Li, J. T. Han, C. A. Wang, H. Xie and J. B. Goodenough, *J. Mater. Chem.*, 2012, **22**, 15357–15361.

27 T. Thompson, A. Sharafi, M. D. Johannes, A. Huq, J. L. Allen, J. Wolfenstine and J. Sakamoto, *Adv. Energy Mater.*, 2015, **5**, 1–9.

28 X. Chen, T. Cao, M. Xue, H. Lv, B. Li and C. Zhang, *Solid State Ionics*, 2018, **314**, 92–97.

29 K. Persson, Materials Data on LiLaO2 (SG:14) by Materials Project, doi:10.17188/1290550, mp-756544, https://materialsproject.org/materials/mp-756544/.